Friction

Review Article

Origin of superlubricity of diamond-like carbon (DLC)

Seokhoon Jang[1], Zhe Chen[2], Seong H. Kim[1,✉]

Cite this article: Jang S, Chen Z, Kim SH. *Friction*, 2025, **13**: 9440995. https://doi.org/10.26599/FRICT.2025.9440995

ABSTRACT: Hydrogenated diamond-like carbon (H-DLC) is typically produced as a coating or thin film through plasma-enhanced chemical vapor deposition (PE-CVD). H-DLC is relatively hard and well known to exhibit superlubricity. Is superlubricity an intrinsic property of H-DLC? This paper argues that H-DLC is not intrinsically superlubricious, but it has an ideal structure that allows transition of the interface region to a superlubricious structure upon frictional shear in proper conditions. Thus, its superlubricity is an extrinsic property. This argument is made by comparing frictional behaviors of three allotropes of carbon materials—graphite, amorphous carbon (a-C), and diamond, and carefully scrutinizing the run-in behavior as well as environment sensitivity of H-DLC friction. The superlubricious structure is generally known to be graphitic, but its exact structure remains elusive and is subject to further study. Nevertheless, accurate knowledge of how superlubricity is induced for H-DLC can guide engineering design to achieve superlubricious behaviors with other carbon materials produced via different synthetic routes.

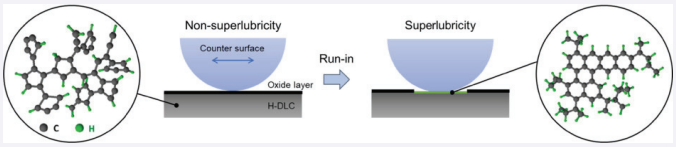

KEYWORDS: superlubricity; diamond-like carbon (DLC); run-in; environmental sensitivity

1 Introduction

Friction plays an important role in almost all aspects of moving systems—both natural and engineering. In some cases, we want friction. Without friction, one cannot grip objects or walk from one location to another. In a brake system, a large friction is necessary to stop the moving vehicle. In other cases, we want to reduce friction. For example, friction causes parasitic energy loss in moving engineering systems [1]. In automobiles with internal combustion engines, only 21% of the energy generated by fuel is actually used for propulsion of the car; out of 79% of energy loss, 17% is due to friction [1–3]. Considering the large number of automobiles around us and in the whole world, it is easy to imagine how significant the energy saving would be if the frictional energy loss is reduced by 1% in the transportation industry alone.

In most engineering systems, friction mitigation is usually done through liquid lubricants or grease, which prevents direct contact between two solid surfaces moving at different speeds [4–6]. But, during the start and stop of motion, the lubricant film is squeezed out, and direct solid–solid contact is inevitable. In that case, boundary lubrication is needed, where solid lubricant coatings may be beneficial for surface protection [7–9]. On the other hand, in microelectromechanical systems or space applications, conventional liquid-based lubricants cannot be used, and friction control should be done through solid lubricants or lubricious coatings [10–14].

Probably, the two most widely used solid lubricants are graphite and MoS_2. One common feature of these two is that they are two-dimensional (2D) layered materials. Under proper environmental conditions, these solid lubricants can provide a low coefficient of friction (COF; μ), protecting the substrate material from wear [15–20]. Especially when COF is close to or even lower than 0.01, the solid lubricant is called "superlubricious" [21, 22]. The basal planes of these layered materials are intrinsically superlubricious due to atomic smoothness and chemical inertness [23–31].

There is another type of solid coating material that can exhibit superlubricity—it is hydrogenated diamond-like carbon (H-DLC), which is typically produced via plasma-enhanced chemical vapor deposition (PE-CVD) methods [32–36]. Figures 1(a) and 1(b) display the very first data showing the superlubricity of H-DLC, published by Erdemir et al. [36] and Donnet et al. [37]. Unlike graphite and MoS_2, H-DLC does not have a well-defined 2D layered structure in the bulk. Instead, it consists of three-dimensional (3D) amorphous carbon (a-C) networks of sp^2 and sp^3-hybridized carbon species with some hydrogen species randomly distributed in the network [38, 39]. Then, how does H-DLC coating with the 3D network structure exhibit the superlubricious behavior that is typically observed at the basal plane of 2D layered materials?

Since the discovery of the superlubricity of H-DLC [40–54], this question has been studied extensively. From phenomenological observations, it was initially proposed that the superlubricity originates from the hydrogen termination of the carbon atoms exposed at the sliding interface (Fig. 1(c)) [33, 55–57].

[1] Department of Chemical Engineering and Materials Research Institute, Pennsylvania State University, University Park, PA 16802, USA. [2] State Key Laboratory of Fluid Power and Mechatronic Systems, Zhejiang University, Hangzhou 310058, China.

✉ Corresponding author. E-mail: shk10@psu.edu

Received: July 17, 2023; Revised: August 21, 2024; Accepted: August 28, 2024

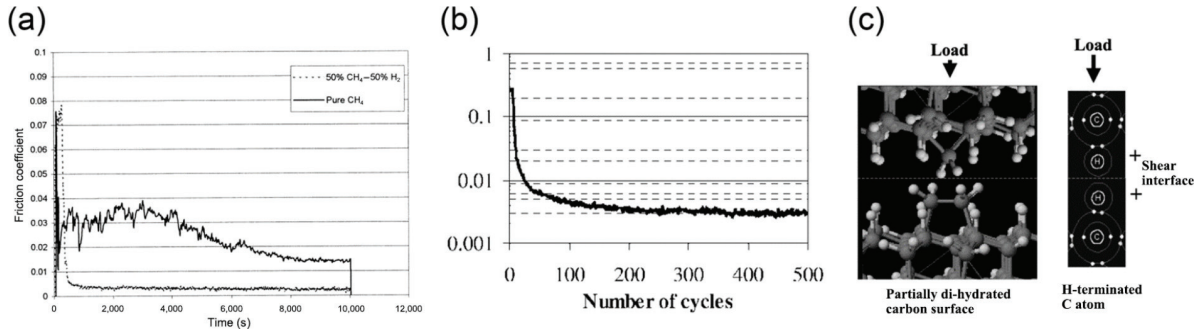

Fig. 1 Superlubricity of H-DLC reported by (a) Erdemir et al. and (b) Donnet et al., and (c) schematic illustration explaining the superlubricity proposed by Erdemir et al. in 2001. In (a), H-DLC films were derived from pure CH_4 and 50% CH_4 + 50% H_2 plasmas, respectively, and the friction tests were conducted in dry nitrogen environment. In (b), H-DLC film was deposited by DC PECVD from acetylene, and the friction tests were performed in an ultra-high vacuum. Reproduced with permission from Ref. [36] for (a), © Elsevier Science S. A. 2020; Ref. [37] for (b), © Plenum Publishing Corporation 2001; Ref. [34] for (c), © Elsevier Science B.V. 2011.

The main supporting evidence for this view comes from the facts that (i) in inert environments (such as high vacuum or dry nitrogen), superlubricity is readily observed for H-DLC with high hydrogen contents but not for H-DLC with low hydrogen contents [33, 36, 49, 54], and (ii) the poorly hydrogenated DLC can also exhibit superlubricity in H_2-containing environments [33, 37, 49]. It was hypothesized that the H-terminated DLC surfaces can be positively charged, and the electrostatic repulsion between these two surfaces could be the origin of superlubricity [58, 59]. Computationally, it was predicted that H-bearing carbon atoms could be slightly positively charged due to the electronegativity difference between H and C [57]. Although H-termination provides the passivation of the carbon surface, it is unlikely that this partial charge plays a significant role in superlubricity.

It should be noted that the basal planes of 2D materials (graphite and MoS_2) exhibit superlubricity immediately as soon as friction test starts, while H-DLC coating surface becomes superlubricious after a run-in period [43, 51, 53, 60–62]. Here, the run-in is the period during which COF is initially high and gradually decreases to a super-low value (≤0.01). Initially, it was thought that the run-in behavior of H-DLC is due to the presence of a layer with non-ideal structures deposited at the end of PE-CVD process (i.e., residual species after the deposition step is ceased) or the adsorption of adventitious hydrocarbon contaminants on H-DLC surface during the sample storage [62–65]. If so, one could argue that the superlubricity of H-DLC is an intrinsic property, which can be observed as soon as the contaminant layer is removed.

If the superlubricity of H-DLC is an intrinsic property specific to a-C network with a proper hydrogen content, an important scientific question arises. One of the most widely used structural analysis methods for a-Cs, including H-DLC, is Raman spectroscopy [46, 48–52, 62, 66–70]. D- and G-band spectral features in 1,300–1,600 cm^{-1} region of Raman spectra provide various structural aspects of H-DLC films, which include the degree of graphitization, graphitic domain size, H-content, density, etc. [71–74]. There are other types of a-C that exhibit Raman spectral features similar to H-DLC but do not show superlubricity [75–77]. Then, what is unique about H-DLC, and why do other types of a-C showing similar Raman spectral features not exhibit superlubricity? If the superlubricity of H-DLC is not an intrinsic property of H-DLC, what causes the H-DLC surface to transform into a superlubricious state? If the superlubricity of H-DLC is an extrinsic property, can superlubricity be achieved with other a-C networks by tuning their structures or properties? These questions are important for both scientific understanding and knowledge-based materials design to engineer friction behaviors of carbon materials.

This review paper compiles and delineates recently published experimental data that collectively suggest that the superlubricity of H-DLC is an extrinsic property induced by external conditions, which include a proper amount of frictional shear applied to the material with proper structures in proper environmental conditions. The key to this thesis is to understand the run-in behavior properly; thus, the chemical and physical processes taking place during the run-in period will be reviewed and cohesively interpreted to draw the argument that the superlubricity of H-DLC is not an intrinsic property but an extrinsic property. From this angle, we can explain why H-DLC can readily exhibit superlubricity. It also helps to devise an engineering strategy to attain superlubricity with other types of a-C.

2 Comparison of friction behaviors of carbon allotropes

Figure 2 schematically compares the structure of graphite, a-C, and diamond and summarizes the typical friction behaviors of these materials reported in the literature. Figure 3 plots COF values of various types of carbon materials found in the literature, along with the Raman spectral features revealing the hybridization structure of carbon in each type of carbon allotropes [32–34, 58, 71, 78–96]. At a quick glance, it can be seen that H-DLC is unique in terms of COF. Let us take a deeper look into each allotrope.

Graphite consists of 2D hexagonal lattices of sp^2-hybridized carbon atoms, which are stacked via van der Waals interactions [97, 98]. Polycrystalline samples containing mostly nano-scale crystallites are specifically called nano-crystalline graphite (NC-G) [99, 100]. A bulk material molded by isostatic compression during graphitization is called isographite [101]. By applying lateral shear during the graphitization at high temperature, highly-oriented pyrolytic graphite (HOPG) is obtained [102, 103]. Diamond has a face-centered cubic (FCC) lattice of sp^3-hydridized carbon atoms. These two allotropes are in thermodynamic equilibrium state. Other crystalline carbon materials are fullerene and carbon nanotubes [104–106], which are not covered in this review.

All other bulk carbon materials without specific long-range order of repeating units fall into the a-C category. These a-C materials have random networks of sp^2- and sp^3-hybridized carbons. Raman spectroscopy is frequently utilized to qualitatively assess the degree of sp^2 and sp^3 hybridizations in a-C materials [48, 49, 73, 107–113]. It should be noted that a-C is a non-

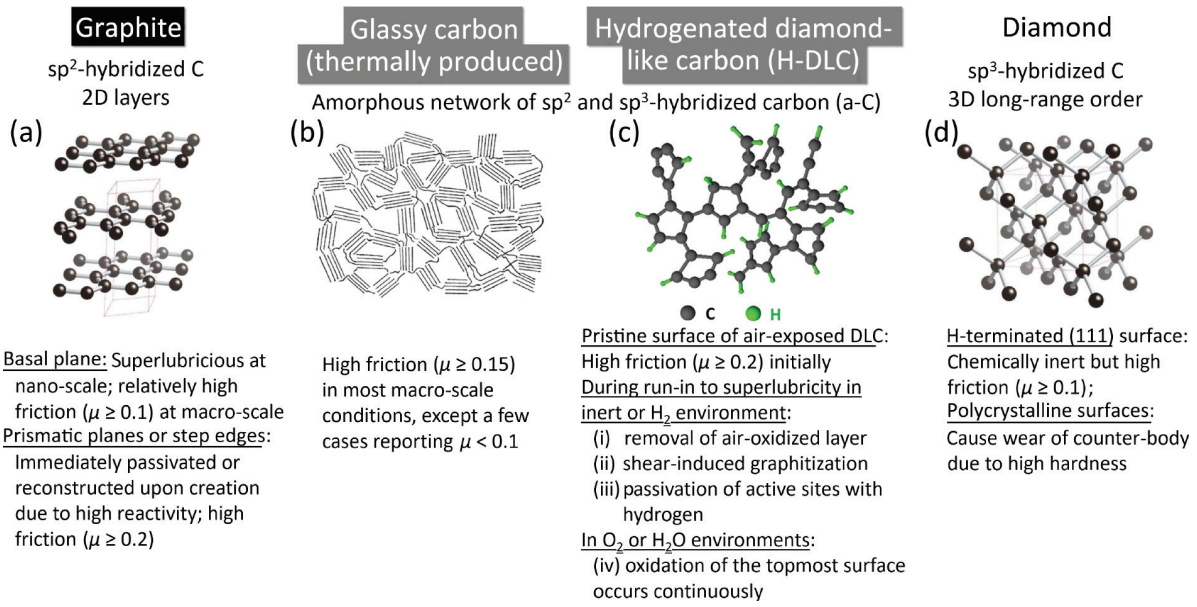

Fig. 2 Atomic structure and typical friction behaviors of (a) graphite, (b) GC, (c) H-DLC, and (d) diamond.

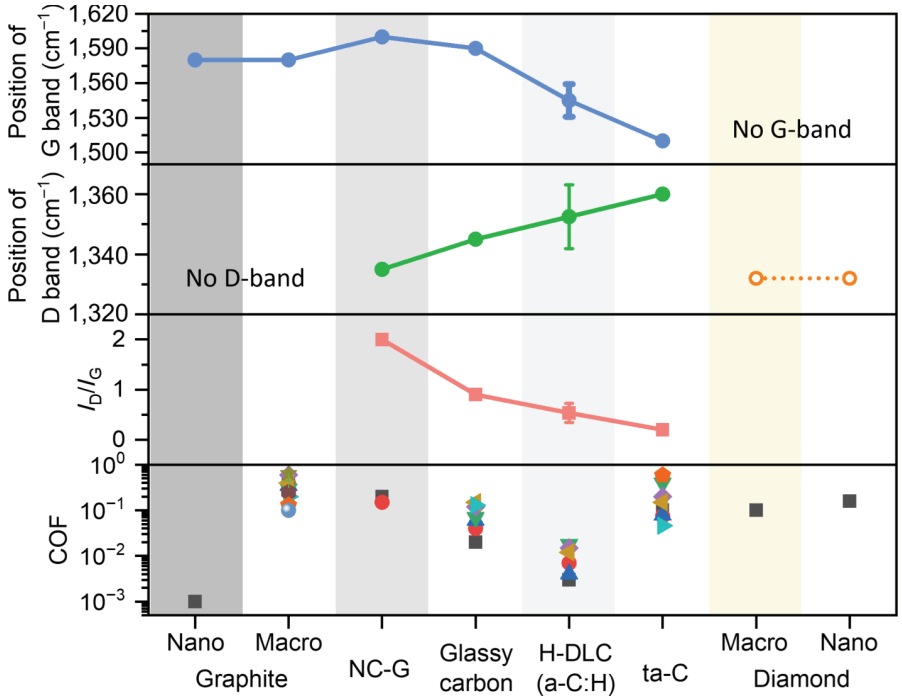

Fig. 3 Comparison of the positions of D and G bands in Raman spectra, the intensity ratio of D to G bands (I_D/I_G), and COF of various carbon materials measured at the macroscale, along with COF measured at the nanoscale for graphite and diamond. NC-G represents nano-crystalline graphite; a-C:H denotes hydrogenated amorphous carbon; ta-C stands for tetrahedral amorphous carbon. Note that the vibrational mode of the D band of diamond (1,332 cm^{-1}) is different from the D-band of graphite and graphitic domains, which is the breathing mode of sp^2-C ring structures.

equilibrium material; it means that its chemical compositions and structures vary if synthesis method or condition is changed [33, 34, 36, 49, 50, 54, 114]. So, each a-C material produced via a different method is unique, even though all of them are described with the same name in the literature. a-C materials produced through pyrolysis of organic precursors are typically called glassy carbon (GC) [115, 116]. Obviously, the pyrolysis temperature of a-C is lower than the full graphitization temperature. The coatings produced via CVD or physical vapor deposition (PVD) are called DLC. Probably, the reason they are called DLC is because they are much harder than GC although not as hard as diamond. The ones with substantial degrees of hydrogenation are specifically referred to as H-DLC. The ones with high sp^3-C content are called tetrahedral amorphous carbon (ta-C). Depending on the precursor gases used for synthesis, other elements can be incorporated in a-C network [117–119].

The friction of the graphite basal plane (including graphene) has been studied extensively [23, 120–125]. While COF measured on the (0001) basal plane of graphite in a nanoscale using atomic force microscopy (AFM) is as low as 0.001 (even lower in even lower in some literatures) [23, 120–122], COFs measured for various graphite-based materials in a macroscopic scale (for

清華大學出版社 Tsinghua University Press | SciOpen

example, using a pin-on-disk tribometer in ambient air) are typically ≥ 0.1, many orders of magnitude larger than the values measured with AFM [78–85, 95, 126]. COFs measured in dry nitrogen or vacuum are higher than those measured in humid air [78–83, 95].

This contact scale dependence must be due to mechanical weakness of graphite; its hardness is only a few GPa for the basal plane [127]. In the macroscopic experiment, the microfracture of the crystallites in the sliding contract region exposes prismatic planes (which consist of step edges). The graphene step edges have much higher friction than the basal plane [27, 128–132]. In AFM experiments, it was found that even a single-layer thick step edge of graphene (i.e., 0.35 nm thick) with the zig–zag structure on the graphite basal plane can increase the local COF from < 0.001 to > 0.1. Figure 4 displays AFM lateral and height signal recorded as a sharp AFM probe (made of silicon, covered with native oxide) ascends and descends a single-layer thick graphene step edge on the graphite basal plane [128]. Although a buckling of the graphene edge had been proposed as a potential source for large friction at the step edge [133], it was found to occur rather rarely [130]. The adhesion force measured at the step edge is obviously larger than that at the basal plane, but its dependence on the distance from the step edge is quite different from (at least does not correlate with) that of friction force [132]. Through detailed comparisons with reactive molecular dynamics (MD) simulations, it was found that the resistive force during the step-down (descending) is due to hydrogen bonding interactions between the native oxide at the tip surface and the OH groups at the graphene step edge, and the step-down assistive force is due to local strain of atoms within the tip caused by the edge topography [128]. The large friction during the step-up (ascending) is due to the synergistic actions of the chemical (hydrogen bonding) and physical (topography) effects [128]. Without the chemical effect, the topography alone does not cause a large increase in friction during the AFM probe sliding [27]. At the graphene step edge with the arm-chair structure, COF is much lower than that of the zig-zag edge, but the arm-chair edges are not abundant [27, 134]. These nanoscale experimental data collectively provide a key insight into the reason that COFs measured for graphite with pin-on-disk instruments are high. The microfracture of the basal plane is difficult to avoid in macroscale friction tests due to the roughness of the counter-surface and a large shear force from the large contact area.

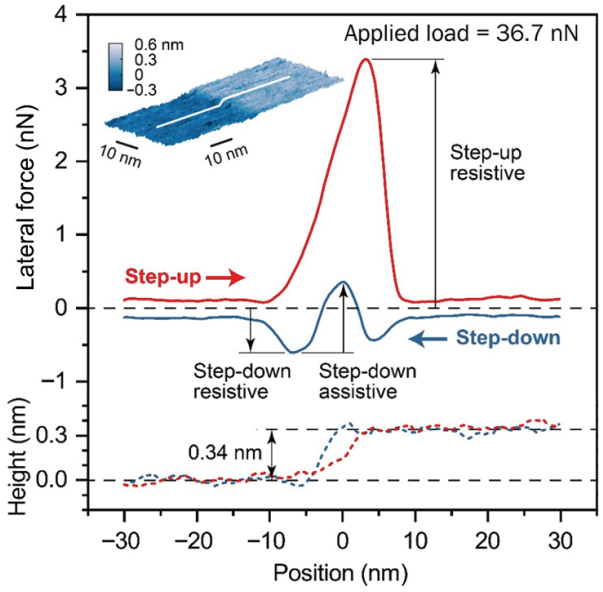

Fig. 4 Lateral force (solid lines) and height profile (dashed lines) measured at a graphene step edge with a silica AFM tip. The normal force applied to the tip was 36.7 nN, and the sliding speed was 500 nm/s. In the step-up direction, the positive lateral force means that the graphene step edge is resisting tip sliding. In the step-down direction, the negative lateral force is resistive to the tip sliding, and the positive (or upward deviation from the negative trend) force is assistive to the tip sliding. The inset is the AFM topographic image of the graphene step edge. The height of the step edge is 0.34 nm, corresponding to the sum of the thickness of one graphene layer and the interlayer spacing between adjacent graphene layers. Reproduced with permission from Ref. [128], © The Authors 2019.

When friction is measured directly on the prismatic planes of graphite, COF is even higher because the areal density of these high-friction edges is much larger [127]. The hardness of the prismatic facets of graphite is less than 1 GPa. Thus, mechanical damage to the surface can readily occur locally, resulting in a large wear. All these detrimental effects can be avoided in the nanoscale experiment with AFM by finding the area where the step edges are absent and measuring friction under the condition where the basal plane structure is unaltered.

The diamond surface provides an ideal platform to test the hydrogen termination hypothesis because the extremely high hardness allows the measurement of COF without surface damage. When single-crystalline diamond facets are terminated with hydrogen, COF measured with AFM or simulated computationally is on the order of 0.1 [135–137]. The fact that the H-terminated diamond surface cannot give COF smaller than 0.1 suggests that the hydrogen passivation mechanism shown in Fig. 1(c) may not be sufficient to fully explain the superlubricity of H-DLC. Also, it is noted that due to the extremely high hardness, diamonds can abrase the counter-surface, especially when polycrystalline surfaces with a large roughness are used in the friction test [138–140]. For that reason, diamond is not a good solid lubricant material.

Similarly, ta-C is not an ideal solid lubricant coating. COF values reported in the literature vary over a wide range, mostly larger than 0.1 (Fig. 3) [87–92]. It has a relatively high hardness [39, 141, 142]. Thus, it may work well for the protection of the surface onto which ta-C coating is applied, but it could cause wear of the counter-surface [143].

Once again, we can see in Fig. 3 that H-DLC is the most promising carbon allotrope for solid lubrication purposes [38, 39]. But it should be noted that H-DLC exhibits superlubricity in the macro-scale friction test always after a brief run-in period, only when it contains enough hydrogen in the film in inert environment or the tribo-test is carried out in H_2-containing environments [58, 93, 94]. It does not exhibit superlubricity in humid air [93, 144–146]. It is very rare to see the superlubricious behavior in the nano-scale test [48, 147]. The following sections summarize mechanistic understanding made so far in regard to this peculiarity in friction of H-DLC.

3 Removal of the air-oxidized surface layer of H-DLC during run-in

Figure 5 displays C 1s spectra of an H-DLC surface with a 40% H-content taken with X-ray photoelectron spectroscopy (XPS) analysis [65]. The sample was stored in air since H-DLC surface does not degrade over time in typical storage conditions in ambient air. In the survey spectrum taken without Ar-ion sputtering, oxygen-to-carbon (O/C) ratio was found to be around 0.15±0.01 [65]. Even if the surface is cleaned with oxygen plasma or ethanol prior to XPS analysis, this ratio does not vary

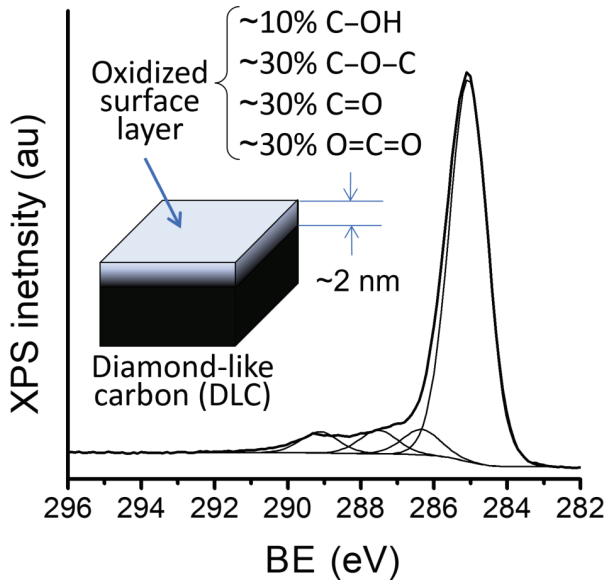

Fig. 5 High-resolution C 1s XPS spectra of H-DLC films cleaned by ethanol rinse. The peaks are fitted with four components—285, 286.5, 287.8, and 289.4 eV with the same peak width. The inset shows the composition of the oxidized surface layer. The deconvolution of C–OH and C–O–C was done through chemical derivatization. Reproduced with permission from Ref. [65], © Elsevier B. V. 2011.

meaningfully, and the spectral components in C 1s region do not change significantly [65, 148]. If the oxygen-containing species originated from adventitious contaminants, the O/C ratio would have been altered upon cleaning. Thus, the oxygen-containing species detected in XPS after proper cleaning must be a constituent part of H-DLC surface.

Since PE-CVD was done in high vacuum with precursors that do not contain oxygen, the oxygen detection in XPS indicates that H-DLC surface undergoes post-synthesis oxidation upon air exposure. It can be viewed as "native oxide" in analogy to those on silicon and metal surfaces. Based on the O/C ratio and the photoelectron escape depth in XPS, the thickness of the oxidized surface layer is estimated to be 1–2 nm [65, 148]. The distribution of the oxidized species could be determined by the combination of peak deconvolution of C 1s XPS spectra and/or chemical derivatizations (Fig. 5) [65].

The surface oxidation of H-DLC upon air exposure is an unavoidable outcome of the nonequilibrium structural distribution of sp^2- and sp^3-hybridized carbon atoms. Since H-DLC is produced via PE-CVD process, which involves the bombardment of high-energy particles and ions, its structure is highly reactive. The hybridization structures of sp^2 and sp^3 carbons deviate from the ideal geometry because they cannot be fully relaxed to the equilibrium structures once they are randomly connected to form a 3D network. In the randomly-connected network, a large fraction of carbon atoms have bond angles and distances inevitably far from the equilibrium geometry. In MD simulations of DLC structure produced by rapid quenching from 6,000 K, the pair-distribution function for the interatomic C–C distance is found to be quite broad [149]. Although the synthesis process is different from experimentally-produced H-DLC, the carbon atoms possessing non-ideal bond lengths and angles must be highly reactive since they are not in the energy minimum (equilibrium) state. For this reason, when H-DLC is retrieved from the deposition chamber, its surface will readily react with oxygen and water molecules impinging from the ambient air.

The fact that the thickness of the air-oxidized layer is only 1–2 nm means that the growth of the native oxide layer is a self-limited process [150]. It is most likely to be limited by the diffusivity of oxygen into the subsurface region at room temperature. As the oxygen or H_2O diffuses into the subsurface region and reacts with carbon atoms that are far from the equilibrium hybridization geometries, the sub-nm scale pores, if they ever exist, may get congested, forming a barrier layer that limits further ingress of oxygen or water species [150]. This is the reason that H-DLC surface does not degrade even after storage in ambient condition for a long time. Obviously, if the sample is heated in air, the oxidized layer thickness can grow further [46, 62].

During the run-in period in inert environments (dry N_2 or vacuum), the air-oxidized layer wears off. This can be supported by the following experimental evidence. The wear depth of H-DLC measured after the run-in period is typically on the order of a few nanometers, which is close to the thickness of the air-oxidized surface layer [63–65]. Once the superlubricious state is reached, the wear rate is extremely low since fiction is extremely small. That means most wear has occurred during the run-in period. When H-DLC is oxidized, the D-band is enhanced and the G-band is slightly blue-shifted (Fig. 6(b)) [46, 62]. This is because the oxidation is accompanied by the enhancement of the graphitic sp^2 carbon fraction [70, 73, 151]. During the run-in period of the thermally-oxidized H-DLC surface, it was observed that the D-band is decreased, and the G-band is slightly red-shifted as the oxidized surface layer wears off (Fig. 6(a)) [46]. More recently, a time-of-flight secondary ion mass spectrometry (ToF-SIMS) analysis was used for oxygen signal mapping and showed that the oxygen content is reduced in the friction-tested region (Fig. 6(c)) [147].

4 Structural changes in the interface region during run-in

From the data discussed in Section 3, we can see that the prerequisite to the superlubricity of H-DLC is the removal of the air-oxidized surface layer. However, it is just a necessary condition, not a sufficient condition. The superlubricity of H-DLC is not readily observed in the nanoscale friction test with a sharp AFM tip even after the wear depth exceeds the thickness of the air-oxidized surface layer [48]. In contrast, superlubricity was observed when a dull AFM tip was used [147]. The main difference between these two was the presence of a carbon deposit on the tip surface. When the tip was sharp, there was no sign of carbon deposits in the apex of the tip [48]; but when the tip was blunt, there was a clear sign of carbon deposits [147]. This carbon deposit on the counter-surface is called a transfer film. Also, in microscale and macroscale friction tests, the superlubricity of H-DLC is always accompanied by the formation of transfer film on the counter-surface, and based on the Raman analysis, the structure of the transfer film is quite different from that of H-DLC [46, 48–51, 53, 152–156]. All these reports suggest that the formation of a "stable" transfer film on the counter-surface during the run-in process plays an important role. It appears that the transfer film prevents direct contact between the two sliding solid surfaces. In that sense, it could be said that, although it is solid, the transfer film formed on the counter-surface by rubbing against H-DLC behaves like a liquid lubricant film in the hydrodynamic lubrication regime in the Stribeck curve. Note that COF at the onset of hydrodynamic lubrication is also ultra-low (typically, μ on the order of 0.01 or even less) [157, 158]. Here, it would be interesting to make an analogy to physical gels, which remain solid-like in their stationary state but flow like a fluid under shear stress [159].

It is important to understand the chemical composition and structure of this superlubricious transfer film; however, such information has been elusive for various reasons. Two immediate reasons are the high reactivity of a-C surface and the detection limit of the technique used. When the sliding track was analyzed *ex situ* with XPS, which has a probe depth on the order of 10 nm, the surface was always subjected to oxidation during the sample transfer from the tribo-tester to the XPS system [50, 62, 160]. In dry air and humid argon environments, the surface condition changes within a few seconds, and the run-in behavior resumes in the subsequent test at the same location (Figs. 7(a) and 7(b)) [160]. Even in a high-purity argon environment that contains only ~10 ppm of oxygen and water, it takes less than 5 min to lose the superlubricity, and the run-in behavior resumes (Fig. 7(c)) [160]. This implies that even if a special suitcase that is pulled to vacuum or filled with inert gas is used for sample transfer, it may not be sufficient to keep the superlubricious H-DLC surface unaltered before the *ex-situ* analysis begins. Again, this attests that H-DLC surface is highly reactive; its reactivity is self-limited to the top surface region (around 1–2 nm thick) due to the transport limit in the subsurface region [150].

For structural analysis, Raman spectroscopy has been extensively used to analyze the sliding track in H-DLC surface after the run-in period [44, 46–50, 61, 64–68]. But, because the probe depth of Raman spectroscopy (typically exceeding several hundred nanometers) [49, 161–163] is larger than the thickness of this superlubricious interface, the measured spectrum is convoluted with the signal from H-DLC underneath the surface. For that reason, the Raman spectral features of the tribo-tested region appear essentially identical to those of the pristine surface, as shown in Fig. 8(a) [49]. The *in-situ* Raman analysis can monitor spectral changes in real-time under the tribo-testing

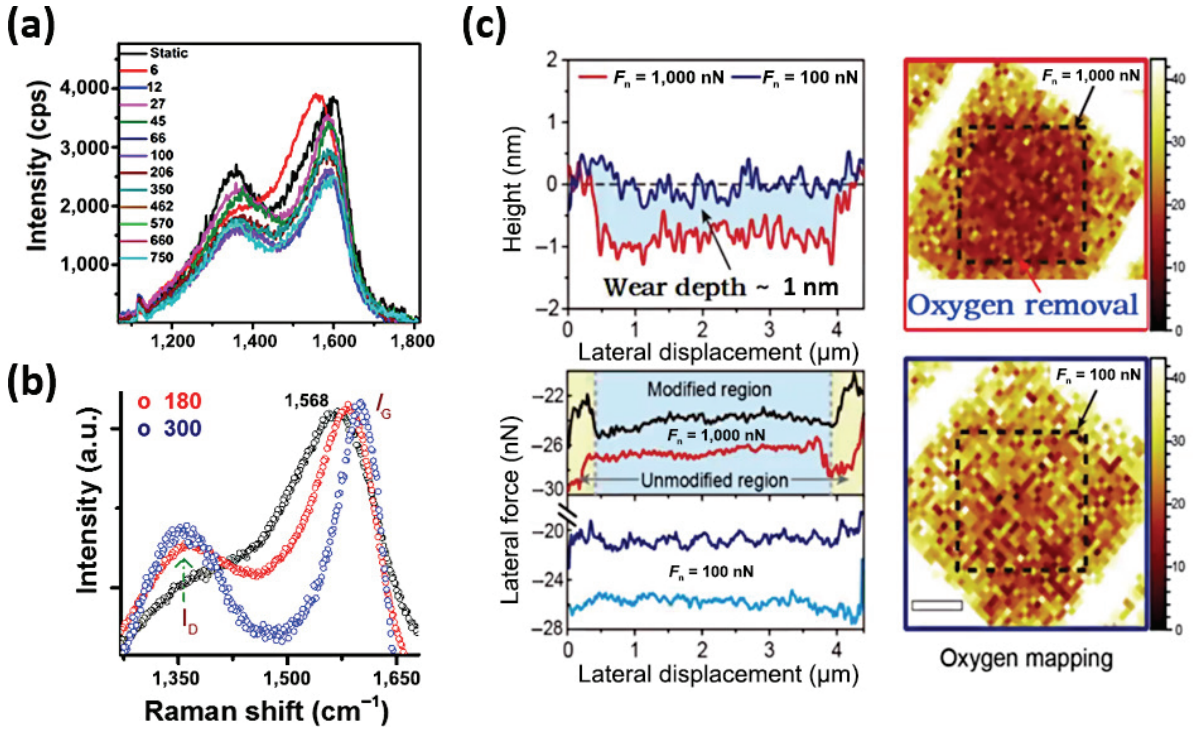

Fig. 6 (a) *In-situ* Raman spectra captured at the sliding interface between a sapphire ball and an H-DLC surface that was thermally pre-oxidized at 300 °C. (b) *Ex-situ* Raman spectra of pristine and thermally-oxidized H-DLC at 180 and 300 °C. (c) Line profiles of H-DLC after sliding at 1,000 and 100 nN, along with their respective lateral force signals. O-mapping images of the wear regions obtained using TOF-SIMS are displayed on the right. Reproduced with permission from Ref. [46] for (a, b), © American Chemical Society 2017; Ref. [147] for (c), © Wiley-VCH GmbH 2020.

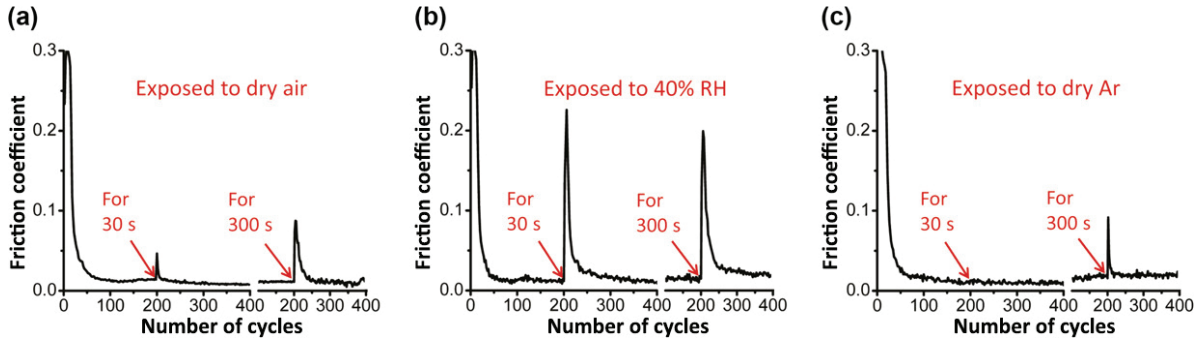

Fig. 7 COF of self-mated H-DLC films as a function of cycle in dry Ar (O_2 < 8 ppm; H_2O < 10 ppm) using a ball-on-disk tribometer. In (a) and (b), the sliding ball was lifted from the substrate after the 200th sliding cycle and then exposed to (a) dry air and (b) Ar with 40% RH for 30 or 300 s, and then the sliding was resumed in dry Ar. In (c), the sliding ball was lifted from the substrate for a period of time while the environment vapor was always dry Ar. Reproduced with permission from Ref. [161], © Elsevier B. V. 2005.

condition, but it still encounters the issue of (or is difficult to deconvolute) the contribution from the bulk H-DLC beneath the sliding interface.

This predicament can be circumvented by analyzing the transfer film on the counter-surface. The frictional interface is not an equilibrium surface. The inherent complication of nonequilibrium thermodynamics is that its property is not a state function but a path-dependent function. But this complication can be used as an advantage—it means that the chemical and structural information of the shear plane during friction is inscribed into the transfer film on the counter-surface; thus, by analyzing the transfer film on the counter-surface of a foreign material (so, not self-mated friction test), one can deduce the chemical and structural information of the sliding interface that is not accessible otherwise. It just needs to be remembered that the degree of oxidation upon air exposure after the friction test may vary depending on the transfer film structure.

Figure 8(b) displays a typical Raman spectra of a transfer film remaining on a stainless-steel ball surface after reaching the steady-state ultra-low COF [49]. The Raman analysis of the transfer films clearly shows an increase in the D- and G-band intensity ratio (I_D/I_G) and a blue shift of G-band position. This suggests that the transfer film (and, thus, the sliding interface) is more graphitic than the pristine H-DLC structure. In fact, the high-resolution transmission electron microscopy (TEM) images of the transfer films often show layered patterns that are parallel to the sliding plane [147, 152, 153]. This must be formed by the action of "frictional shear stress" [157, 158].

There appears to be a critical threshold for the shear-induced graphitization to occur (Fig. 9) [147]. When the contact pressure is low, the run-in process takes longer (i.e., more reciprocating cycles are needed). When the contact pressure is high, the frictional force is also high, and the run-in cycle is relatively short. In nanoscale testing with a blunt AFM tip, the threshold contact stress was found to be ~1.35 GPa [147]. In macroscale tests, the threshold stress is much lower; for example, superlubricity is readily observed even at an average Hertzian contact pressure of ~230 MPa [48].

TEM has been used to analyze the cross-section of the surface region in the sliding track on H-DLC or the transfer film [147, 152, 153]. Many of these TEM images show a few nm thick "layered structure" regions in which multiple lamellae lie parallel to the sliding direction. These features also indicate that the sliding interface is "graphitic". But, the exact nature is not known. The layered feature does not necessarily mean that they are graphene or graphene oxide layers. Similarly, reactive MD simulations also suggested some degree of graphitization of carbon structures within the sliding interface [149, 164–166].

5 Role of hydrogen on H-DLC superlubricity

In addition to the removal of the air-oxidized layer and the shear-induced graphitization, the degree of hydrogenation of the transfer film (which reflects the chemistry of the shear plane region) also plays a very important role. The degree of hydrogenation can be estimated by comparing the fluorescence background in the Raman spectra with an empirical correlation function [49, 107, 167]. Note that this is just an approximation. Since the empirical equation was produced with bulk H-DLC coatings with different hydrogen contents, the effect of surface oxidized layer in the Raman spectral features is quite small. In contrast, the transfer film on the counter-surface could be porous, and thus, the degree of oxidation could be high. The effect of oxidation by air on the Raman signal background has not been studied systematically [168]. Nonetheless, a qualitative comparison could still be possible.

For H-DLC coating with an H-content of 40%, the superlubricious transfer film always shows a high degree of hydrogenation—very close to the maximum H-content (which is about 40% due to stoichiometric and structural constraints in H-DLC) [48, 49]. In contrast, H-DLC with a lower H-content (for example, 30%) shows high friction in N_2 after the initial run-in and its transfer film was less graphitic and poorly hydrogenated [33, 49, 169, 170]. It is known that if the poorly-hydrogenated H-DLC is tested in H_2-containing environments, ultra-low COF can be achieved after a brief run-in period [31, 35, 47]. Figure 10 schematically compares the Raman spectral features measured for the transfer films formed from H-DLC with 30% H-content retrieved at various stages of the run-in period. The transfer film formed in dry nitrogen, which gives high friction, shows the spectral features of low degree of graphitization and low hydrogen concentration. In contrast, the transfer film formed in H_2-containing gas exhibits the spectral features of more graphitic and highly hydrogenated species [49]. Considering the crucial role of hydrogen in the structural rearrangement of DLC network [171], future research could focus more on the correlation between hydrogen content and the degree of graphitization.

The role of hydrogenation is thought to be the passivation of

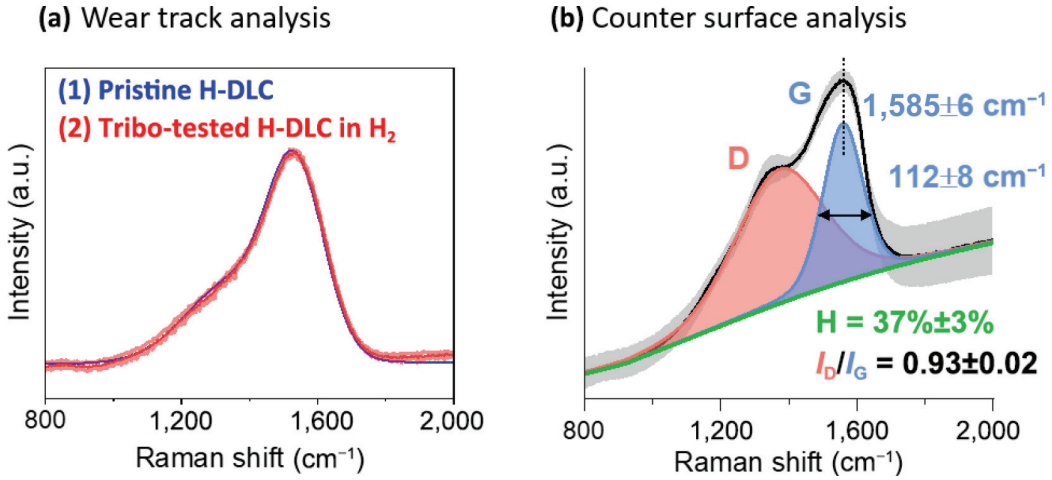

Fig. 8 (a) Raman spectra of pristine H-DLC with an H-content of 30% and its sliding track produced in an H_2 gas environment; (b) transfer film formed on a stainless-steel counter ball after sliding in H_2. Reproduced with permission from Ref. [49], © Elsevier Ltd. 2022.

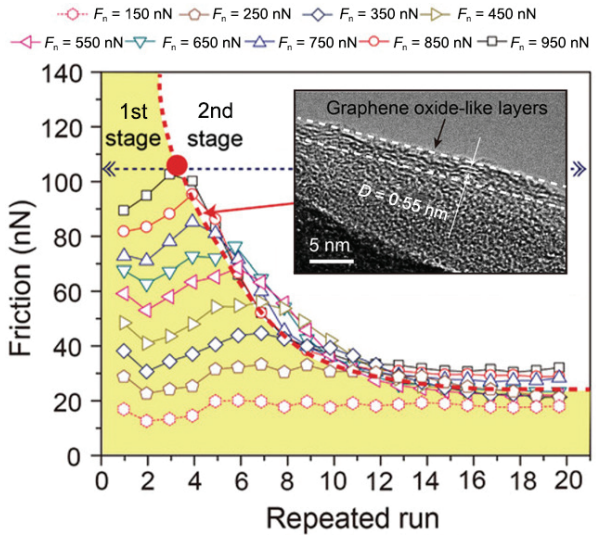

Fig. 9 Friction evolution of an AFM tip sliding on an H-DLC film at different applied normal loads. The two typical stages of running-in are divided by the red dotted line. The inset is an HR-TEM image of the blunted tip apex after running-in, showing the formation of an extremely thin layer with a total thickness of ~2 nm and an interlayer spacing of ~0.55 nm, which is consistent with the layer spacing of graphene oxide. Reproduced with permission from Ref. [147], © Wiley-VCH GmbH 2020.

the reactive sites. Similar to the graphene step edges (Fig. 4), the edges of the graphitic domains could cause high friction. During the frictional sliding, some dangling bonds could be produced due to local tribochemical dissociation of C–C and C–H bonds. If they are not properly passivated, they can form C–C covalent bonds across the shear interface, which will lead to high friction and high wear. When H-DLC contains a sufficiently large amount of hydrogen, endogenous hydrogen species could be available to passivate such reactive sites. If the degree of hydrogenation is not high enough (as in the case of H-DLC with a 30% H-content), such passivation effects can be induced by keeping a sufficiently high partial pressure of H_2 in the test environment [31, 35, 47].

6 Environmental effect on H-DLC superlubricity

There is a plethora of literature reporting the loss of the superlubricity of H-DLC due to the presence of O_2 and/or H_2O in the testing environment [91, 140–142]. Again, this environment sensitivity originates from the chemical reactivity of carbon species whose bond length and angle deviate from the equilibrium sp^2 and sp^3 hybridization [50]. By modeling the effect of O_2 and H_2O partial pressure on COF with a Langmuir-type kinetics derived for tribochemical processes taking place within the sliding contact and during the time between consecutive sliding cycles, one can estimate the probability of the topmost H-DLC surface freshly exposed by frictional wear to react with molecules impinging from the gas phase [47, 50].

Figure 11 compares the reaction rate constant obtained for two H-DLC coatings (30% and 40% H-content) as a function of partial pressures of H_2O and O_2 [50]. The oxidation probability (a) of 30% and 40% H-DLCs in O_2 and H_2O environments is on the order of 10^{-4}–10^{-2} $kPa^{-1}{\cdot}s^{-1}$. These values are quite comparable, magnitude-wise, to the hydrogenation reaction probability of unsaturated hydrocarbons on highly-reactive noble metal catalysts such as Pt and Pd (around 10^{-2} $kPa^{-1}{\cdot}s^{-1}$) [172–174]. In both H-DLC cases, $a(H_2O)$ is 3–4 times larger than $a(O_2)$. This difference could be ascribed to the higher sticking coefficient of H_2O molecules [175, 176] than O_2. Unlike O_2, H_2O can have hydrogen bonding interactions among physisorbed molecules and thus a longer residence time at the surface.

It is also interesting to note that the oxidized surface species formed by reaction with O_2 are highly susceptible to tribochemical wear, and thus, the overall wear rate increases as the O_2 partial pressure increases. In contrast, the water molecules physisorbed at the sliding surface act like a molecular lubrication layer; thus, although COF in humid nitrogen is higher than that in dry air, the wear rate in humid nitrogen is lower than that in dry air [47, 50]. In high humidity conditions, the adsorbed water layer can act like a "liquid" film and cause galvanic corrosion of dissimilar material contact [177]. Although H-DLC is an insulator, the shear-induced graphitic layer can be conductive. Since graphite is highly

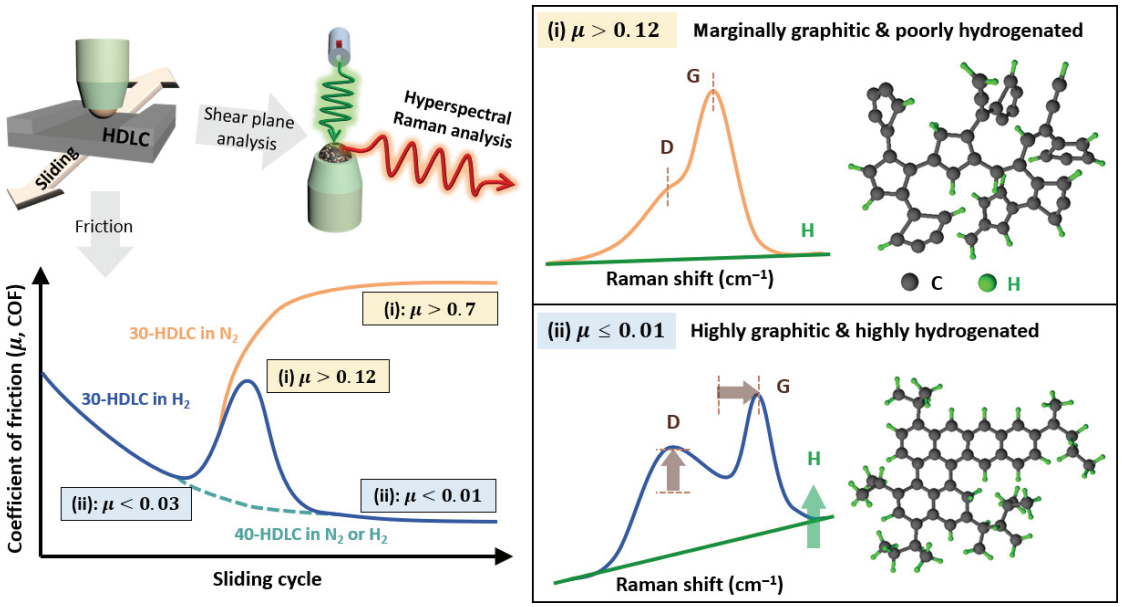

Fig. 10 Schematics illustrating the distinct frictional periods of H-DLCs hydrogenated at 30% and 40% in N_2 and H_2 gas environments, along with the evolution of Raman spectral features of the corresponding transfer films formed on a counter ball. This depicts the correlation between friction and the degree of graphitization and hydrogenation at the sliding interface. Reproduced with permission from Ref. [49], © Elsevier Ltd. 2022.

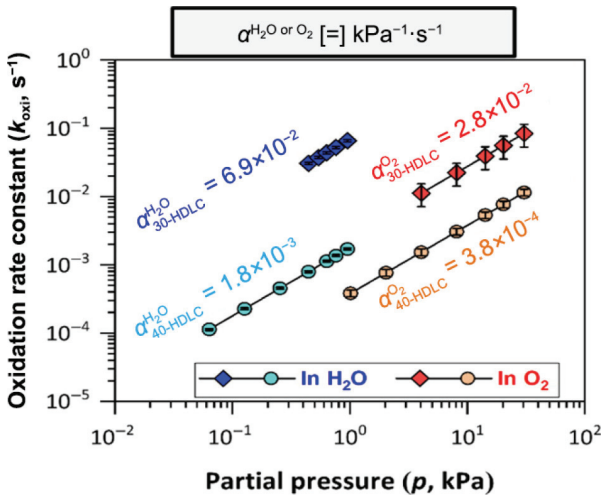

Fig. 11 Oxidation rate constants (α) of H-DLCs with 30% and 40% hydrogen content in the coating varying with the partial pressures of H_2O and O_2 (P_{H_2O} and P_{O_2}), determined by fitting the sliding cycle-dependent COF of H-DLC under various P_{H_2O} and P_{O_2} using a Langmuir-type kinetics model. Reproduced with permission from Ref. [50], © American Chemical Society 2023.

cathodic, the anodic counter surface (such as stainless steel) can be corroded in the presence of liquid water. This leads to severe wear of the metallic counter-surface and negligible wear of H-DLC in high humidity conditions [177].

Recently, it was also found that molecules physisorbed on the silica counter-surface and dragged into the interface between the silica and the graphite basal plane could alter the friction behavior [31, 178]. When an AFM tip covered with a native oxide layer is slid on the graphite basal plane, a small degree of stick-slip behavior can be observed (Fig. 12(a)). When pentanol is adsorbed, it can reduce the stick-slip behavior, making the interface more lubricious (Fig. 12(b)) [31]. In contrast, when phenol or water molecules are adsorbed, the stick-slip behavior can be amplified (Figs. 12(c) and 12(d)) [31]. It is speculated that such amplification effects are due to commensurate interactions between the molecules adsorbed on the silica surface and the 2D lattice of the graphite basal plane [31]. Something similar could occur more readily at the shear-induced graphitic planes in the sliding interface of H-DLC and the counter-surface. If so, this could be another possible mechanism contributing to the environmental sensitivity of H-DLC friction.

7 Summary and perspective

Putting together the experimental evidence discussed so far, it becomes clear that the superlubricity of H-DLC is not an intrinsic property of the hydrogen-terminated topmost surface of the amorphous network consisting of randomly-connected sp^2 and sp^3 carbons (Fig. 1(c)). If it is an intrinsic property, it would not be sensitive to the test conditions. COF of H-terminated diamond surface is about 0.1. COF of ultrahigh molecular-weight polyethylene is also around 0.1 and 0.15, although its sliding surface has C–H terminations [179]. COF of these materials is not sensitive to environmental conditions as long as there is no severe wear. Thus, the superlubricity of H-DLC must be an extrinsic interfacial property induced by friction in certain environmental conditions. As shown in Fig. 13, the prerequisite conditions for the superlubricity of H-DLC are (i) removal of the air-oxidized surface layer (which would be tribochemical processes), (ii) shear-induced graphitization of the interface region, and (iii) proper passivation of graphitic domains by hydrogen. The exact nature of the "shear-induced graphitic" domain in the transfer film remains elusive. They could be turbostratic, at least locally [95, 180–183]. When a cross-sectional region of a transfer film was imaged with TEM, a very thin layer of multiple lamellae aligned parallel to the

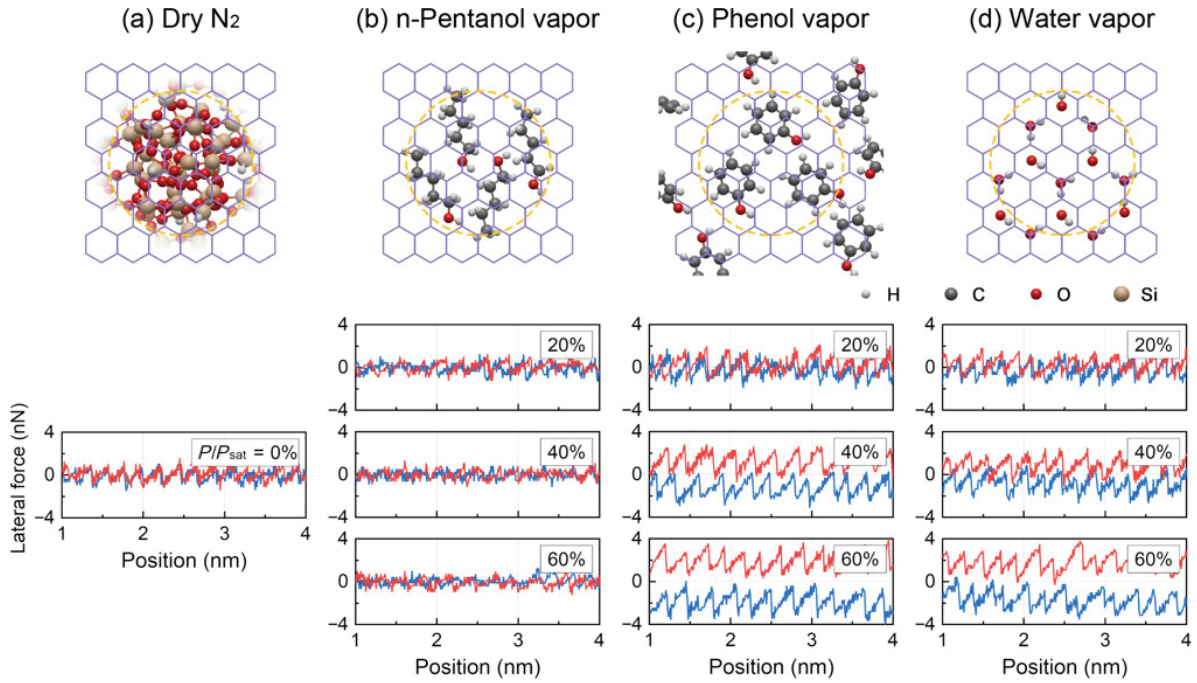

Fig. 12 Nanoscale friction behavior of a silica AFM tip (applied load = 6.5 nN) sliding on graphite basal plane recorded in (a) dry nitrogen, (b) n-pentanol vapor, (c) phenol vapor, and (d) water vapor at ambient pressure and ambient temperature. The upper panel schematically shows the atomic arrangements in the sliding interface, where vapor molecules adsorbed on the silica are projected to the graphite basal plane. The lower panels show the lateral force recorded during the contact scan, indicating that the contact commensuration is influenced by the adsorbed molecules. The relative partial pressure (P/P_{sat}) indicates the concentration of the gas species while the background is dry nitrogen. Reproduced with permission from Ref. [31], © Elsevier Ltd. 2022.

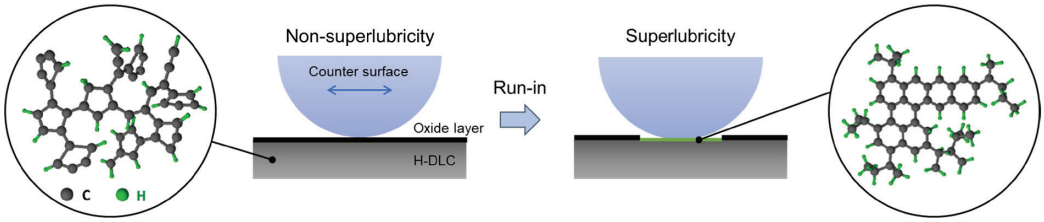

Fig. 13 Schematic illustration of the surface condition on H-DLC during run-in leading to superlubricity. H-DLC is of amorphous sp^2- and sp^3-carbon network and has a native oxide layer on it (black colored). During the run-in, the oxidized surface layer wears off, and a more graphitic structure with passivation with hydrogen at all reactive sites is formed due to frictional shear in the sliding interface (green-colored).

shear direction is often observed, which has been interpreted as the presence of "graphitic" or "graphene-like" layers. However, it is also difficult to firmly rule out the possibility that such graphitic features are produced by high-energy electron beam damage during TEM analysis. If they are not something caused by the beam damage, then the parallel alignment of the lamellae along the shear direction might be the fourth prerequisite [184]. Another important prerequisite (which could be the fifth) is that the shear-induced graphitic domains should always remain within the sliding contact (via adhering to the counter-surface). When the contact area is extremely small (such as a contact scan with a sharp AFM tip), the shear-induced graphitic domains are continuously pushed out (probably because the adhesion force is too small as compared to the friction force), and the sliding occurs between the H-DLC surface against the fresh counter-surface.

Knowing that the superlubricity of H-DLC is a friction-induced extrinsic property, one could ask the following question—why is superlubricity readily observed for H-DLC but not for other a-C materials that have even more graphitic structures? Maybe the governing factor is the mechanical property. The shear-induced graphitization requires a certain threshold. If the bulk cannot support the applied load, the sliding interface will continuously be subjected to abrasive wear. H-DLC with a 40% H-content has a hardness (H) of ~7–8 GPa and an elastic modulus (E) of ~55–70 GPa [78–85, 95]. H-DLC with a 30% H-content has H = ~20 GPa and E = ~200 GPa [32, 39, 46, 54, 59]. In contrast, GCs have H = 3–4 GPa and E = 30–35 GPa [185]. The poor mechanical properties may be an Achilles' heel of GC materials. In order to have the shear-induced graphitization at the sliding interface, the bulk phase should be able to sustain the applied load so that sufficient frictional shear stress can be generated at the sliding interface. If the bulk is mechanically too weak, then abrasive wear will continuously take place at the sliding interface. Note that the run-in period means the shear-induced graphitization requires repeated sliding [147], it cannot occur instantaneously during the first sliding cycle.

If this view is right, one strategy to attain superlubricity from GC is to enhance its mechanical strength. In fact, GCs are brittle and fracture very easily; they can be porous as well. If one could make GC mechanically stronger—by reducing porosity or filling pores with secondary materials, or by doping with other elements, etc.—it might be possible to improve the lubricity. Although most literatures that studied tribological properties of GCs reported relatively high friction ($\mu > 0.1$) [78–85, 95], a few papers reported a COF less than 0.1 (in some cases, as low as 0.02) [78–80]. However, the experimental details were not well described in those old papers. Maybe those old studies might have achieved something unique (mechanically strong) without recognizing the importance of that trait.

Another possibility could be residual oxygen. Since H-DLC is produced using oxygen-free precursors in high vacuum conditions, the incorporation of oxygen species in the bulk phase is very unlikely. Since GCs are produced from organic precursors containing not just carbon and hydrogen but other elements, including oxygen, they are likely to contain residual oxygen species unless the pyrolysis temperature is increased to the full graphitization temperature. The trace amount of oxygen may have an impact on how low COF of GCs can be [184]. If this is a dominant factor, an engineering strategy is to use a precursor that would leave a lower level of residual oxygen species.

Since GC films are made at high temperatures and then cooled to room temperature, the adhesion to the substrate may be weak if the coefficient of thermal expansion (CTE) of the substrate is significantly different from that of GC. Thus, the substrate materials should be chosen properly to match CTE of GC. CTE of GC is around 2–5 ppm/K [185–187]. This means that superlubricious GCs could be produced on ceramic surfaces that have low CTEs but not on metal surfaces with large CTEs. In that case, PE-CVD of H-DLC would be a better option to mitigate the friction problem.

Acknowledgements

This work is a cumulative outcome of a series of projects funded by the Air Force Office of Scientific Research (No. FA9550-08-1-0010) and the National Science Foundation (Nos. CMMI-1131128, 1727571, 1912199, and 2315343). The authors acknowledge the previous students who worked on these projects and, especially, Prof. Ali Erdemir, who collaborated with us and provided H-DLC samples when he was at the Argonne National Laboratory.

Declaration of competing interest

The authors have no competing interests to declare that are relevant to the content of this article. The author Seong H. Kim is the Editorial Board Member of this journal.

References

[1] Holmberg K, Erdemir A. Influence of tribology on global energy consumption, costs and emissions. *Friction* **5**(3): 263–284 (2017)

[2] Holmberg K, Andersson P, Nylund N O, Mäkelä K, Erdemir A. Global energy consumption due to friction in trucks and buses. *Tribol Int* **78**: 94–114 (2014)

[3] Holmberg K, Erdemir A. The impact of tribology on energy use and CO_2 emission globally and in combustion engine and electric cars. *Tribol Int* **135**: 389–396 (2019)

[4] Rawat S S, Harsha A P. Current and future trends in grease lubrication. In: *Automotive Tribology*. Katiyar J K, Bhattacharya S, Patel V K, Kumar V, Eds. Singapore: Springer Singapore, 2019: 147–182.

[5] Bhat S A, Charoo M S. Effect of additives on the tribological properties of various greases—A review. *Mater Today Proc* **18**: 4416–4420 (2019)

[6] Chen Y, Jha S, Raut A, Zhang W Y, Liang H. Performance characteristics of lubricants in electric and hybrid vehicles: A review of current and future needs. *Front Mech Eng* **6**: 571464 (2020)

[7] Martin J M, Grossiord C, Le Mogne T, Igarashi J. Transfer films and friction under boundary lubrication. *Wear* **245**(1–2): 107–115 (2000)

[8] Persson B N J. Theory of friction and boundary lubrication. *Phys Rev B* **48**(24): 18140–18158 (1993)

[9] Zahid R, Hassan M B H, Varman M, Mufti R A, Kalam M A, Zulkifli N W B M, Gulzar M. A review on effects of lubricant formulations on tribological performance and boundary lubrication mechanisms of non-doped DLC/DLC contacts. *Crc Cr Rev Sol State* **42**(4): 267–294 (2017)

[10] Lince J R. Effective application of solid lubricants in spacecraft mechanisms. *Lubricants* **8**(7): 74 (2020)

[11] Roberts E W. Thin solid lubricant films in space. *Tribol Int* **23**(2): 95–104 (1990)

[12] Kim S H, Asay D B, Dugger M T. Nanotribology and mems. *Nano Today* **2**(5): 22–29 (2007)

[13] Maboudian R, Carraro C. Surface chemistry and tribology of mems. *Annu Rev Phys Chem* **55**: 35–54 (2004)

[14] Williams J A, Le H R. Tribology and mems. *J Phys D Appl Phys* **39** (12): R201–R214 (2006)

[15] Furlan K P, de Mello J D B, Klein A N. Self-lubricating composites containing MoS_2: A review. *Tribol Int* **120**: 280–298 (2018)

[16] Donnet C, Martin J M, Le Mogne T, Belin M. Super-low friction of MoS_2 coatings in various environments. *Tribol Int* **29**(2): 123–128 (1996)

[17] Savan A, Pflüger E, Voumard P, Schröer A, Simmonds M. Modern solid lubrication: Recent developments and applications of MoS_2. *Lubr Sci* **12**(2): 185–203 (2000)

[18] Vazirisereshk M R, Martini A, Strubbe D A, Baykara M Z. Solid lubrication with MoS_2: A review. *Lubricants* **7**(7): 57 (2019)

[19] Kumar N, Dash S, Tyagi A K, Raj B. Super low to high friction of turbostratic graphite under various atmospheric test conditions. *Tribol Int* **44**(12): 1969–1978 (2011)

[20] Anand G, Saxena P. A review on graphite and hybrid nano-materials as lubricant additives. *Iop Conf Ser-Mat Sci* **149**: 012201 (2016)

[21] Luo J B, Zhou X. Superlubricitive engineering—Future industry nearly getting rid of wear and frictional energy consumption. *Friction* **8**(4): 643–665 (2020)

[22] Hirano M, Shinjo K. Superlubricity and frictional anisotropy. *Wear* **168**(1–2): 121–125 (1993)

[23] Dienwiebel, M, Verhoeven G S, Pradeep N, Frenken J W M, Heimberg J A, Zandbergen H W. Superlubricity of graphite. *Phys Rev Lett* **92**: 126101 (2004).

[24] Verhoeven G S, Dienwiebel M, Frenken J W M. Model calculations of superlubricity of graphite. *Phys Rev B* **70**(16): 165418 (2004)

[25] Feng X F, Kwon S, Park J Y, Salmeron M. Superlubric sliding of graphene nanoflakes on graphene. *ACS Nano* **7**(2): 1718–1724 (2013)

[26] van Wijk M M, Dienwiebel M, Frenken J W M, Fasolino A. Superlubric to stick-slip sliding of incommensurate graphene flakes on graphite. *Phys Rev B* **88**(23): 235423 (2013)

[27] Chen L, Chen Z, Tang X Y, Yan W M, Zhou Z R, Qian L M, Kim S H. Friction at single-layer graphene step edges due to chemical and topographic interactions. *Carbon* **154**: 67–73 (2019)

[28] Chen Z, Khajeh A, Martini A, Kim S H. Identifying physical and chemical contributions to friction: A comparative study of chemically inert and active graphene step edges. *ACS Appl Mater Inters* **12**: 30007–30015 (2020)

[29] Chen Z, Khajeh A, Martini A, Kim S H. Origin of high friction at graphene step edges on graphite. *ACS Appl Mater Inter* **13**: 1895–1902 (2021)

[30] Chen Z, Khajeh A, Martini A, Kim S H. Chemical and physical origins of friction on surfaces with atomic steps. *Sci Adv* **5**: eaaw0513 (2019)

[31] Chen Z, Kim S H. Tuning super-lubricity via molecular adsorption. *Applied Materials Today* **29**: 101615 (2022)

[32] Erdemir A, Eryilmaz O L, Nilufer I B, Fenske G R. Synthesis of superlow-friction carbon films from highly hydrogenated methane plasmas. *Surf Coat Tech* **133–134**: 448–454 (2000)

[33] Erdemir A. The role of hydrogen in tribological properties of diamond-like carbon films. *Surf Coat Tech* **146–147**: 292–297 (2001)

[34] Johnson J A, Woodford J B, Rajput D, Kolesnikov A I. Carbon-hydrogen bonding in near-frictionless carbon. *Appl Phys Lett* **93**: 131911 (2008)

[35] Erdemir A, Nilufer I B, Eryilmaz O L, Beschliesser M, Fenske G R. Friction and wear performance of diamond-like carbon films grown in various source gas plasmas. *Surf Coat Tech* **120–121**: 589–593 (1999)

[36] Erdemir A, Eryilmaz O L, Nilufer I B, Fenske G R. Effect of source gas chemistry on tribological performance of diamond-like carbon films. *Diam Relat Mater* **9**(3–6): 632–637 (2000)

[37] Donnet C, Fontaine J, Grill A, Le Mogne T. The role of hydrogen on the friction mechanism of diamond-like carbon films. *Tribol Lett* **9**(3–4): 137–142 (2001)

[38] Donnet C, Erdemir A. *Tribology of Diamond-Like Carbon Films: Fundamentals and Applications*. New York (USA): Springer, 2007.

[39] Erdemir A, Donnet C. Tribology of diamond-like carbon films: Recent progress and future prospects. *J Phys D Appl Phys* **39**(18): R311 (2006)

[40] Semenov A P, Khrushchov M M. Influence of environment and temperature on tribological behavior of diamond and diamond-like coatings. *J Frict Wear+* **31**(2): 142–158 (2010)

[41] Zeng Q F, Ning Z K. High-temperature tribological properties of diamond-like carbon films: A review. *Rev Adv Mater Sci* **60**: 276–292 (2021)

[42] Erdemir A, Fontaine J, Donnet C. An overview of superlubricity in diamond-like carbon films. In: *Tribology of Diamond-Like Carbon Films*. Donnet C, Erdemir A, Eds. New York: Springer, 2008: 237–262.

[43] Liu Y H, Jiang Y L, Sun J H, Wang L, Liu Y Q, Chen L, Zhang B, Qian L M. Durable superlubricity of hydrogenated diamond-like carbon film against different friction pairs depending on their interfacial interaction. *Appl Surf Sci* **560**: 150023 (2021)

[44] Liu Y H, Yu B J, Cao Z Y, Shi P F, Zhou N N, Zhang B, Zhang J Y, Qian L M. Probing superlubricity stability of hydrogenated diamond-like carbon film by varying sliding velocity. *Appl Surf Sci* **439**: 976–982 (2018)

[45] Wang D L, Gong Z B, Jiang B Z, Yu G M, Liu G Q, Wang N. Structure original of temperature depended superlow friction behavior of diamond like carbon. *Diam Relat Mater* **107**: 107880 (2020)

[46] Manimunda P, Al-Azizi A, Kim S H, Chromik R R. Shear-induced structural changes and origin of ultralow friction of hydrogenated diamond-like carbon (DLC) in dry environment. *ACS Appl Mater Inter* **9**: 16704–16714 (2017)

[47] Jang S, Chen Z, Kim S H. Environmental effects on superlubricity of hydrogenated diamond-like carbon: Understanding tribochemical kinetics in O_2 and H_2O environments. *Appl Surf Sci* **580**: 152299 (2022)

[48] Jang S, Colliton A G, Flaih H S, Irgens EMK, Kramarczuk L J, Rauber GD, Vickers J, Ogrinc A L, Zhang Z X, Gong Z B, et al. Why is superlubricity of diamond-like carbon rare at nanoscale. *Small* **20**: 2400513 (2024)

[49] Jang S, Kim S H. Distinct effects of endogenous hydrogen content and exogenous hydrogen supply on superlubricity of diamond-like carbon. *Carbon* **202**: 61–69 (2023)

[50] Jang S, Rabbani M, Ogrinc A L, Wetherington M T, Martini A, Kim S H. Tribochemistry of diamond-like carbon: Interplay between hydrogen content in the film and oxidative gas in the environment. *ACS Appl Mater Inter* **15**(31): 37997–38007 (2023)

[51] Scharf T W, Singer I L. Monitoring transfer films and friction instabilities with *in situ* Raman tribometry. *Tribol Lett* **14**: 3–8 (2003)

[52] Scharf T W, Singer I L. Quantification of the thickness of carbon transfer films using Raman tribometry. *Tribol Lett* **14**(2): 137–145 (2003)
[53] Scharf T W, Singer I L. Role of the transfer film on the friction and wear of metal carbide reinforced amorphous carbon coatings during run-in. *Tribol Lett* **36**: 43–53 (2009)
[54] Jeng Y R, Islam S, Wu K T, Erdemir A, Eryilmaz O. Investigation of nano-mechanical and tribological properties of hydrogenated diamond like carbon (DLC) coatings. *J Mech* **33**: 769–776 (2016)
[55] Bernal R A, Chen P, Harrison J A, Jeng Y R, Carpick R W. Influence of chemical bonding on the variability of diamond-like carbon nanoscale adhesion. *Carbon* **128**: 267–276 (2018)
[56] Gao G T, Mikulski P T, Chateauneuf G M, Harrison J A. The effects of film structure and surface hydrogen on the properties of amorphous carbon films. *J Phys Chem B* **107**(40): 11082–11090 (2003)
[57] Piotrowski P L, Cannara R J, Gao G T, Urban J J, Carpick R W, Harrison J A. Atomistic factors governing adhesion between diamond, amorphous carbon and model diamond nanocomposite surfaces. *J Adhes Sci Technol* **24**(15–16): 2471–2498 (2010)
[58] Erdemir A, Eryilmaz O. Achieving superlubricity in DLC films by controlling bulk, surface, and tribochemistry. *Friction* **2**: 140–155 (2014)
[59] Erdemir A. Genesis of superlow friction and wear in diamondlike carbon films. *Tribol Int* **37**(11–12): 1005–1012 (2004)
[60] Cui L C, Lu Z B, Wang L P. Environmental effect on the load-dependent friction behavior of a diamond-like carbon film. *Tribol Int* **82**: 195–199 (2015)
[61] Andersson J, Erck R A, Erdemir A. Friction of diamond-like carbon films in different atmospheres. *Wear* **254**: 1070–1075 (2003)
[62] Al-Azizi A A, Eryilmaz O, Erdemir A, Kim S H. Surface structure of hydrogenated diamond-like carbon: Origin of run-in behavior prior to superlubricious interfacial shear. *Langmuir* **31**: 1711–1721 (2015)
[63] Mangolini F, McClimon J B, Rose F, Carpick R W. Accounting for nanometer-thick adventitious carbon contamination in X-ray absorption spectra of carbon-based materials. *Anal Chem* **86**: 12258–12265 (2014)
[64] Mehta N J, Roy S, Johnson J A, Woodford J, Zinovev A, Islam Z, Erdemir A, Sinha S, Fenske G, Prorok B. X-ray studies of near-frictionless carbon films. *MRS Online Proceedings Library* **843**: 271–276 (2004)
[65] Yang M, Marino M J, Bojan V J, Eryilmaz O L, Erdemir A, Kim S H. Quantification of oxygenated species on a diamond-like carbon (DLC) surface. *Appl Surf Sci* **257**(17): 7633–7638 (2011)
[66] Okubo H, Sasaki S, Lancon D, Jarnias F, Thiébaut B. Tribo-Raman-SLIM observation for diamond-like carbon lubricated with fully formulated oils with different wear levels at DLC/steel contacts. *Wear* **454–455**: 203326 (2020)
[67] Liu Y H, Zhang B, Chen L, Cao Z Y, Shi P F, Liu J W, Zhang J Y, Qian L M. Perspectives of the friction mechanism of hydrogenated diamond-like carbon film in air by varying sliding velocity. *Coatings* **8**(10): 331 (2018)
[68] Kataria S, Dhara S, Barshilia H C, Dash S, Tyagi A K. Evolution of coefficient of friction with deposition temperature in diamond like carbon thin films. *J Appl Phys* **112**(2): 023525 (2012)
[69] Liu Y H, Wang L, Liu T, Zhang P. Effect of normal loads and mating pairs on the tribological properties of diamond-like carbon film. *Wear* **486–487**: 204083 (2021)
[70] Irmer G, Dorner-Reisel A. Micro-raman studies on DLC coatings. *Adv Eng Mater* **7**(8): 694–705 (2005)
[71] Ferrari A C. Non-destructive characterisation of carbon films. In: *Tribology of Diamond-Like Carbon Films: Fundamentals and Applications*. Donnet C, Erdemir A, Eds. New York (USA): Springer, 2007: 25–82.
[72] Rose F, Wang N, Smith R, Xiao Q F, Inaba H, Matsumura T, Saito Y, Matsumoto H, Dai Q, Marchon B, et al. Complete characterization by Raman spectroscopy of the structural properties of thin hydrogenated diamond-like carbon films exposed to rapid thermal annealing. *J Appl Phys* **116**(12): 123516 (2014)
[73] Ferrari A C, Robertson J. Interpretation of Raman spectra of disordered and amorphous carbon. *Phys Rev B* **61**: 14095 (2000)
[74] Yu Q Y, Chen X C, Zhang C H, Zhang C X, Deng W L, Wang Y H, Xu J X, Qi W. Ion energy-induced nanoclustering structure in a-C: H film for achieving robust superlubricity in vacuum. *Friction* **10** (12): 1967–1984 (2022)
[75] Peng Y, Zhong F S, Qian L M, Jiang S L. Effects of ultraviolet/ozone irradiation on glassy-like carbon film for the bioMEMS applications. *Appl Surf Sci* **533**: 147443 (2020)
[76] Li K S, Xu G, Wen X B, Zhou J, Gong F. High-temperature friction behavior of amorphous carbon coating in glass molding process. *Friction* **9**(6): 1648–1659 (2021)
[77] Chen J S, Sun Z, Lau S P, Tay B K. Structural and tribological properties of hard carbon film synthesized by heat-treatment of a polymer on graphite substrate. *Thin Solid Films* **389**(1–2): 161–166 (2001)
[78] Hokao M, Hironaka S, Suda Y, Yamamoto Y. Friction and wear properties of graphite/glassy carbon composites. *Wear* **237**(1): 54–62 (2000)
[79] Csapo E, Zaidi H, Paulmier D. Friction behaviour of a graphite–graphite dynamic electric contact in the presence of argon. *Wear* **192**: 151–156 (1996)
[80] Mangalick M C. Frictional behavior of commercial graphites. *Carbon* **12**(5): 573–576 (1974)
[81] Bhowmick S, Banerji A, Alpas A T. Role of humidity in reducing sliding friction of multilayered graphene. *Carbon* **87**: 374–384 (2015)
[82] Liu Y B, Lim S C, Ray S, Rohatgi P K. Friction and wear of aluminium–graphite composites: The smearing process of graphite during sliding. *Wear* **159**(2): 201–205 (1992)
[83] Wang L, Tieu A K, Zhu H T, Deng G Y, Hai G J, Wang J, Yang J. The effect of expanded graphite with sodium metasilicate as lubricant at high temperature. *Carbon* **159**: 345–356 (2020)
[84] Chromik R R, Winfrey A L, Lüning J, Nemanich R J, Wahl K J. Run-in behavior of nanocrystalline diamond coatings studied by *in situ* tribometry. *Wear* **265**(3–4): 477–489 (2008)
[85] Radhika R, Kumar N, Sankaran K J, Dumpala R, Dash S, Ramachandra Rao M S, Arivuoli D, Tyagi A K, Tai N H, Lin I N. Extremely high wear resistance and ultra-low friction behaviour of oxygen-plasma-treated nanocrystalline diamond films. *J Phys D Appl Phys* **46**(42): 425304 (2013)
[86] Ferrari A C, Rodil S E, Robertson J. Interpretation of infrared and Raman spectra of amorphous carbon nitrides. *Physl Rev B* **67**: 155306 (2003)
[87] Deng X R, Kousaka H, Tokoroyama T, Umehara N. Tribological behavior of tetrahedral amorphous carbon (ta-C) coatings at elevated temperatures. *Tribol Int* **75**: 98–103 (2014)
[88] Jang Y J, Kim J I, Lee W Y, Kim J. Friction properties of thick tetrahedral amorphous carbon coating with different surface defects under dry contact conditions. *Appl Surf Sci* **550**: 149332 (2021)
[89] Bhowmick S, Banerji A, Khan M Z U, Lukitsch M J, Alpas A T. High temperature tribological behavior of tetrahedral amorphous carbon (ta-C) and fluorinated ta-C coatings against aluminum alloys. *Surf Coat Tech* **284**: 14–25 (2015)
[90] Konicek A R, Grierson D S, Sumant A V, Friedmann T A, Sullivan J P, Gilbert P U P A, Sawyer W G, Carpick R W. Influence of surface passivation on the friction and wear behavior of ultrananocrystalline diamond and tetrahedral amorphous carbon thin films. *Phys Rev B* **85**: 155448 (2012)
[91] Mustafa M M B, Umehara N, Tokoroyama T, Murashima M, Shibata A, Utsumi Y, Moriguchi H. Effect of mesh structure of tetrahedral amorphous carbon (ta-C) coating on friction and wear properties under base-oil lubrication condition. *Tribol Int* **147**: 105557 (2020)
[92] Li X, Murashima M, Umehara N. Effect of nanoparticles as lubricant additives on friction and wear behavior of tetrahedral amorphous carbon (ta-C) coating. *Jurnal Tribologi* **16**: 15–29 (2018)

[93] Sanchez-Lopez J C, Erdemir A, Donnet C, Rojas T C. Friction-induced structural transformations of diamondlike carbon coatings under various atmospheres. *Surf Coat Tech* **163–164**: 444–450 (2003)
[94] Chen Z, He X, Xiao C, Kim S H. Effect of humidity on friction and wear—A critical review. *Lubricants* **6**(3): 74 (2018)
[95] Morstein C E, Klemenz A, Dienwiebel M, Moseler M. Humidity-dependent lubrication of highly loaded contacts by graphite and a structural transition to turbostratic carbon. *Nat Commun* **13**: 5958 (2022)
[96] Chen X C, Li J J. Superlubricity of carbon nanostructures. *Carbon* **158**: 1–23 (2020)
[97] Terrones M, Botello-Méndez A R, Campos-Delgado J, López-Urías F, Vega-Cantú Y I, Rodríguez-Macías F J, Elías A L, Muñoz-Sandoval E, Cano-Márquez A G, Charlier J C. Graphene and graphite nanoribbons: Morphology, properties, synthesis, defects and applications. *Nano Today* **5**(4): 351–372 (2010)
[98] Allen M J, Tung V C, Kaner R B. Honeycomb carbon: A review of graphene. *Chem Rev* **110**(1): 132–145 (2010)
[99] Chu P K, Li L H. Characterization of amorphous and nanocrystalline carbon films. *Mater Chem Phys* **96**(2–3): 253–277 (2006)
[100] Gruen D M. Nanocrystalline diamond films. *Annu Rev Mater Sci* **29**: 211–259 (1999)
[101] Jäger H, Frohs W. *Industrial Carbon and Graphite Materials: Raw Materials, Production and Applications*. Boschstr (Germany): WILEY-VCH GmbH, 2021.
[102] Moore A. Highly-oriented pyrolytic graphite. *Chemistry and Physics of Carbon* **11**: 70 (1973)
[103] Chatterjee S, Kim N Y, Pugno N M, Biswal M, Cunning B V, Goo M, Jin S, Lee S H, Lee Z, Ruoff R S. Synthesis of highly oriented graphite films with a low wrinkle density and near-millimeter-scale lateral grains. *Chem Mater* **32**(7): 3134–3143 (2020)
[104] Dinadayalane T C, Leszczynski J. Remarkable diversity of carbon–carbon bonds: Structures and properties of fullerenes, carbon nanotubes, and graphene. *Struct Chem* **21**(6): 1155–1169 (2010)
[105] Georgakilas V, Perman J A, Tucek J, Zboril R. Broad family of carbon nanoallotropes: Classification, chemistry, and applications of fullerenes, carbon dots, nanotubes, graphene, nanodiamonds, and combined superstructures. *Chem Rev* **115**(11): 4744–4822 (2015)
[106] Li Z, Liu Z, Sun H Y, Gao C. Superstructured assembly of nanocarbons: Fullerenes, nanotubes, and graphene. *Chem Rev* **115** (15): 7046–7117 (2015)
[107] Casiraghi C, Piazza F, Ferrari A C, Grambole D, Robertson J. Bonding in hydrogenated diamond-like carbon by Raman spectroscopy. *Diam Relat Mater* **14**: 1098–1102 (2005)
[108] Benedek G, Milani P, Ralchenko V G. *Nanostructured Carbon for Advanced Applications*. Dordrecht (UK): Springer, 2001.
[109] Ferrari A C, Robertson J. Raman spectroscopy of amorphous, nanostructured, diamond–like carbon, and nanodiamond. *Philos T Roy Soc A* **362**(1824): 2477–2512 (2004)
[110] Cui W G, Lai Q B, Zhang L, Wang F M. Quantitative measurements of sp3 content in DLC films with Raman spectroscopy. *Surf Coat Tech* **205**(7): 1995–1999 (2010)
[111] Zhang L, Wei X, Lin Y, Wang F. A ternary phase diagram for amorphous carbon. *Carbon* **94**: 202–213 (2015)
[112] Lajaunie L, Pardanaud C, Martin C, Puech P, Hu C, Biggs M J, Arenal R. Advanced spectroscopic analyses on a:C–H materials: Revisiting the EELS characterization and its coupling with multi-wavelength Raman spectroscopy. *Carbon* **112**: 149–161 (2017)
[113] Merlen A, Buijnsters J G, Pardanaud, C. A guide to and review of the use of multiwavelength raman spectroscopy for characterizing defective aromatic carbon solids: From graphene to amorphous carbons. *Coatings* **7**(10): 153 (2017).
[114] Bustillo K C, Petrich M A, Reimer J A. Characterization of amorphous hydrogenated carbon using solid-state nuclear magnetic resonance spectroscopy. *Chem Mater* **2**: 202–205 (1990)
[115] Uskoković V. A historical review of glassy carbon: Synthesis, structure, properties and applications. *Carbon Trends* **5**: 100116 (2021)
[116] Sharma S. Glassy carbon: A promising material for micro- and nanomanufacturing. *Materials* **11**(10): 1857 (2018)
[117] Ray S C, Pong W F, Papakonstantinou P. Iron, nitrogen and silicon doped diamond like carbon (DLC) thin films: A comparative study. *Thin Solid Films* **610**: 42–47 (2016)
[118] Safaie P, Eshaghi A, Bakhshi S R. Structure and mechanical properties of oxygen doped diamond-like carbon thin films. *Diam Relat Mater* **70**: 91–97 (2016)
[119] Wang J J, Pu J B, Zhang G G, Wang L P. Tailoring the structure and property of silicon-doped diamond-like carbon films by controlling the silicon content. *Surf Coat Tech* **235**: 326–332 (2013)
[120] Filleter T, McChesney J L, Bostwick A, Rotenberg E, Emtsev K V, Seyller T, Horn K, Bennewitz R. Friction and dissipation in epitaxial graphene films. *Phys Rev Lett* **102**(8): 086102 (2009)
[121] Schwarz U D, Zwörner O, Köster P, Wiesendanger R. Quantitative analysis of the frictional properties of solid materials at low loads. I. Carbon compounds. *Phys Rev B* **56**(11): 6987–6996 (1997)
[122] Li J J, Li J F, Luo J B. Superlubricity of graphite sliding against graphene nanoflake under ultrahigh contact pressure. *Adv Sci* **5**(11): 1800810 (2018)
[123] Lee C G, Li Q Y, Kalb W, Liu X Z, Berger H, Carpick R W, Hone J. Frictional characteristics of atomically thin sheets. *Science* **328** (5974): 76–80 (2010)
[124] Lee C G, Wei X D, Li Q Y, Carpick R, Kysar J W, Hone J. Elastic and frictional properties of graphene. *Phys Status Solidi B* **246** (11–12): 2562–2567 (2009)
[125] Egberts P, Han G H, Liu X Z, Charlie Johnson A T, Carpick R W. Frictional behavior of atomically thin sheets: Hexagonal-shaped graphene islands grown on copper by chemical vapor deposition. *ACS Nano* **8**(5): 5010–5021 (2014)
[126] Gardos M N, Davis P S, Meldrum G R. Crystal-structure-controlled tribological behavior of carbon-graphite seal materials in partial pressures of helium andhydrogen. II. SEM tribometry. *Tribol Lett* **3**: 185–198 (1997)
[127] Xiao J K, Zhang L, Zhou K C, Li J G, Xie X L, Li Z Y. Anisotropic friction behaviour of highly oriented pyrolytic graphite. *Carbon* **65**: 53–62 (2013)
[128] Chen Z, Khajeh A, Martini A, Kim S H. Chemical and physical origins of friction on surfaces with atomic steps. *Sci Adv* **5**(8): eaaw0513 (2019)
[129] Chen Z, Khajeh A, Martini A, Kim S H. Identifying physical and chemical contributions to friction: A comparative study of chemically inert and active graphene step edges. *ACS Appl Mater Inter* **12**(26): 30007–30015 (2020)
[130] Chen Z, Khajeh A, Martini A, Kim S H. Origin of high friction at graphene step edges on graphite. *ACS Appl Mater Inter* **13**(1): 1895–1902 (2021)
[131] Chen Z, Kim S H. Measuring nanoscale friction at graphene step edges. *Friction* **8**(4): 802–811 (2020)
[132] Chen Z, Vazirisereshk M R, Khajeh A, Martini A, Kim S H. Effect of atomic corrugation on adhesion and friction: A model study with graphene step edges. *J Phys Chem Lett* **10**(21): 6455–6461 (2019)
[133] Hunley D P, Flynn T J, Dodson T, Sundararajan A, Boland M J, Strachan D R. Friction, adhesion, and elasticity of graphene edges. *Phys Rev B* **87**: 035417 (2013)
[134] Wang Y F, Guo J M, Gao K X, Zhang B, Liang A M, Zhang J Y. Understanding the ultra-low friction behavior of hydrogenated fullerene-like carbon films grown with different flow rates of hydrogen gas. *Carbon* **77**: 518–524 (2014)
[135] Gao G T, Cannara R J, Carpick R W, Harrison J A. Atomic-scale friction on diamond: A comparison of different sliding directions on (001) and (111) surfaces using MD and AFM. *Langmuir* **23**(10): 5394–5405 (2007)
[136] Harrison J A, White C T, Colton R J, Brenner D W. Molecular-

dynamics simulations of atomic-scale friction of diamond surfaces. *Physl Rev B* **46**: 9700–9708 (1992)
[137] Wang J J, Wang F, Li J M, Sun Q, Yuan P F, Jia Y. Comparative study of friction properties for hydrogen- and fluorine-modified diamond surfaces: A first-principles investigation. *Surf Sci* **608**: 74–79 (2013).
[138] Silva F J G, Casais R B, Martinho R P, Baptista A P M. Role of abrasive material on micro-abrasion wear tests. *Wear* **271**(9–10): 2632–2639 (2011)
[139] Jana A, Dandapat N, Das M, Balla V K, Chakraborty S, Saha R, Mallik A K. Severe wear behaviour of alumina balls sliding against diamond ceramic coatings. *B Mater Sci* **39**(2): 573–586 (2016)
[140] Sharma N, Kumar N, Dhara S, Dash S, Bahuguna A, Kamruddin M, Tyagi A K, Raj B. Tribological properties of ultra nanocrystalline diamond film-effect of sliding counterbodies. *Tribol Int* **53**: 167–178 (2012)
[141] Lemoine P, Quinn J P, Maguire P, McLaughlin J A. Comparing hardness and wear data for tetrahedral amorphous carbon and hydrogenated amorphous carbon thin films. *Wear* **257**(5–6): 509–522 (2004)
[142] Martínez E, Andújar J L, Polo M C, Esteve J, Robertson J, Milne W I. Study of the mechanical properties of tetrahedral amorphous carbon films by nanoindentation and nanowear measurements. *Diam Relat Mater* **10**(2): 145–152 (2001)
[143] Lim M S, Jang Y J, Kim J K, Kim J H, Kim S S. A study on friction and wear properties of tetrahedral amorphous carbon coatings on various counterpart materials. *Tribology and Lubricants* **34**(6): 241–246 (2018)
[144] Kim H I, Lince J R, Eryilmaz O L, Erdemir A. Environmental effects on the friction of hydrogenated DLC films. *Tribol Lett* **21**: 51–56 (2006)
[145] Li H X, Xu T, Wang C B, Chen J M, Zhou H D, Liu H W. Humidity dependence on the friction and wear behavior of diamond-like carbon film in air and nitrogen environments. *Diam Relat Mater* **15**: 1585–1592 (2006)
[146] Li H X, Xu T, Wang C B, Chen J M, Zhou H D, Liu H W. Tribochemical effects on the friction and wear behaviors of a-C: H and a-C films in different environment. *Tribol Int* **40**(1): 132–138 (2007)
[147] Wang K, Zhang J, Ma T B, Liu Y M, Song A S, Chen X C, Hu Y Z, Carpick R W, Luo J B. Unraveling the friction evolution mechanism of diamond-like carbon film during nanoscale running-in process toward superlubricity. *Small* **17**(1): 2005607 (2021)
[148] Marino M J, Hsiao E, Chen Y S, Eryilmaz O L, Erdemir A, Kim S H. Understanding run-in behavior of diamond-like carbon friction and preventing diamond-like carbon wear in humid air. *Langmuir* **27**(20): 12702–12708 (2011)
[149] Li K J, Zhang H, Li G Y, Zhang J L, Bouhadja M, Liu Z J, Skelton A A, Barati M. ReaxFF molecular dynamics simulation for the graphitization of amorphous carbon: A parametric study. *J Chem Theory Comput* **14**(5): 2322–2331 (2018)
[150] Campbell C T. Transition metal oxides: Extra thermodynamic stability as thin films. *Phys Rev Lett* **96**: 066106 (2006)
[151] Ferrari A C, Kleinsorge B, Morrison N A, Hart A, Stolojan V, Robertson J. Stress reduction and bond stability during thermal annealing of tetrahedral amorphous carbon. *J Appl Phys* **85**(10): 7191–7197 (1999)
[152] Merkle A P, Erdemir A, Eryilmaz O L, Johnson J A, Marks L D. *In situ* TEM studies of tribo-induced bonding modifications in near-frictionless carbon films. *Carbon* **48**(3): 587–591 (2010)
[153] Chen X C, Zhang C H, Kato T, Yang X A, Wu S D, Wang R, Nosaka M, Luo J B. Evolution of tribo-induced interfacial nanostructures governing superlubricity in a-C: H and a-C: H: Si films. *Nat Commun* **8**: 1675 (2017)
[154] Neidhardt J, Hultman L, Broitman E, Scharf T W, Singer I L. Structural, mechanical and tribological behavior of fullerene-like and amorphous carbon nitride coatings. *Diam Relat Mater* **13**(10): 1882–1888 (2004)
[155] Singer I L. How third-body processes affect friction and wear. *MRS Bull* **23**(6): 37–40 (1998)
[156] Singer I L, Dvorak S D, Wahl K J. Investigation of thrid body processes by *in-vivo* raman tribometry. *Vtt Symp* **200**: 31–44 (1999)
[157] Guo F, Wang Z X, Liu Y, Wang Y M, Tian Y. Investigation of ultra-low friction between self-mated Si_3N_4 in water after running-in. *Tribol Int* **115**: 365–369 (2017)
[158] Zhang S M, Zhang C H, Li K, Luo J B. Investigation of ultra-low friction on steel surfaces with diketone lubricants. *RSC Adv* **8**(17): 9402–9408 (2018)
[159] Putz A M V, Burghelea T I. The solid–fluid transition in a yield stress shear thinning physical gel. *Rheol Acta* **48**(6): 673–689 (2009)
[160] Marino M J, Hsiao E, Chen Y S, Eryilmaz O L, Erdemir A, Kim S H. Understanding run-in behavior of diamond-like carbon friction and preventing diamond-like carbon wear in humid air. *Langmuir* **27**(20): 12702–12708 (2011)
[161] Harima H. Raman scattering characterization on SiC. *Microelectron Eng* **83**(1): 126–129 (2006)
[162] Cao F C, He Z. Determination of thermal conductivity using micro-Raman spectroscopy with a three-dimensional heating model. *J Raman Spectrosc* **50**(12): 1969–1976 (2019)
[163] Pappas D L, Saenger K L, Bruley J, Krakow W, Cuomo J J, Gu T, Collins R W. Pulsed laser deposition of diamond-like carbon films. *J Appl Phys* **71**: 5675–5684 (1992)
[164] Ma T B, Hu Y Z, Wang H. Molecular dynamics simulation of shear-induced graphitization of amorphous carbon films. *Carbon* **47**(8): 1953–1957 (2009)
[165] Li X W, Wang A Y, Lee K R. Insights on low-friction mechanism of amorphous carbon films from reactive molecular dynamics study. *Tribol Int* **131**: 567–578 (2019)
[166] Zhang J, Wang Y, Chen Q, Su Y X, Xu J X, Ootani Y, Ozawa N, Adachi K, Kubo M. Graphitization dynamics of DLC under water lubrication revealed by molecular dynamics simulation. *J Comput Chem Jpn* **18**(2): 103–104 (2019)
[167] Casiraghi C, Ferrari A C, Robertson J. Raman spectroscopy of hydrogenated amorphous carbons. *Phys Rev B* **72**(8): 085401 (2005)
[168] Abdallah W A, Yang Y. Raman spectrum of asphaltene. *Energ Fuel* **26**(11): 6888–6896 (2012).
[169] Fontaine J, Belin M, Le Mogne T, Grill A. How to restore superlow friction of DLC: The healing effect of hydrogen gas. *Tribol Int* **37** (11–12): 869–877 (2004)
[170] Fontaine J, Donnet C, Grill A, LeMogne T. Tribochemistry between hydrogen and diamond-like carbon films. *Surf Coat Tech* **146–147**: 286–291 (2001)
[171] Chen W Q, Wang K, Miao X R, Zhang J, Song A S, Chen X C, Luo J B, Ma T B. Ultralow-friction at cryogenic temperature induced by hydrogen correlated quantum effect. *Small* **20**(32): 2400083 (2024)
[172] Hagen J. *Industrial Catalysis: A Practical Approach*. Boschstr (Germany): Wiley-VCH Verlag GmbH & Co. KGaA, 2015.
[173] Yoshida H, Koizumi K, Boero M, Ehara M, Misumi S, Matsumoto A, Kuzuhara Y, Sato T, Ohyama J, Machida M. High turnover frequency CO–NO reactions over Rh overlayer catalysts: A comparative study using Rh nanoparticles. *J Phys Chem C* **123**(10): 6080–6089 (2019)
[174] Panagiotopoulou P. Hydrogenation of CO_2 over supported noble metal catalysts. *Appl CataL A-Gen* **542**: 63–70 (2017)
[175] Böttcher A, Niehus H. Oxygen adsorbed on oxidized Ru(0001). *Phys Rev B* **60**(20): 14396–14404 (1999)
[176] Carosella C A, Comas J. Oxygen sticking coefficients on clean (111) silicon surfaces. *Surf Sci* **15**(2): 303–312 (1969)
[177] Alazizi A, Draskovics A, Ramirez G, Erdemir A, Kim S H. Tribochemistry of carbon films in oxygen and humid environments: Oxidative wear and galvanic corrosion. *Langmuir* **32**(8): 1996–2004 (2016)
[178] Khajeh A, Chen Z, Kim S H, Martini A. Effect of ambient chemistry on friction at the basal plane of graphite. *ACS Appl Mater Inter* **11** (43): 40800–40807 (2019)
[179] Cho D H, Bhushan B, Dyess J. Mechanisms of static and kinetic friction of polypropylene, polyethylene terephthalate, and high-

density polyethylene pairs during sliding. *Tribol Int* **94**: 165–175 (2016)
[180] Toth P. Nanostructure quantification of turbostratic carbon by HRTEM image analysis: State of the art, biases, sensitivity and best practices. *Carbon* **178**: 688–707 (2021)
[181] Farbos B, Weisbecker P, Fischer H E, Da Costa J P, Lalanne M, Chollon G, Germain C, Vignoles G L, Leyssale J M. Nanoscale structure and texture of highly anisotropic pyrocarbons revisited with transmission electron microscopy, image processing, neutron diffraction and atomistic modeling. *Carbon* **80**: 472–489 (2014)
[182] Ong T S, Yang H. Effect of atmosphere on the mechanical milling of natural graphite. *Carbon* **38**: 2077–2085 (2000)
[183] Huang J Y, Yasuda H, Mori H. Highly curved carbon nanostructures produced by ball-milling. *Chem Phys Lett* **303**(1–2): 130–134 (1999)
[184] Chen X C, Yin X, Qi W, Zhang C H, Choi J, Wu S D, Wang R, Luo J B. Atomic-scale insights into the interfacial instability of superlubricity in hydrogenated amorphous carbon films. *Sci Adv* **6** (13): eaay1272 (2020)
[185] He Z, Song J L, Lian P F, Zhang D Q, Liu Z J. Excluding molten fluoride salt from nuclear graphite by SiC/glassy carbon composite coating. *Nucl Eng Technol* **51**(5): 1390–1397 (2019)
[186] Marques F C, Lacerda R G, Champi A, Stolojan V, Cox D C, Silva S R P. Thermal expansion coefficient of hydrogenated amorphous carbon. *Appl Phys Lett* **83**(15): 3099–3101 (2003)
[187] Ben J, Martinotto A L, Rech G L, Zorzi J E, Perottoni C A. Thermal expansion of continuous random networks of carbon. *J Non-Cryst Solids* **576**: 121260 (2022)

Seokhoon Jang earned his B.S. degree in 2016 and M.S. degree in 2018, both in chemical engineering from Inha University, Republic of Korea. In 2019, he began his Ph.D. in chemical engineering at Penn State, USA, under the supervision of Prof. Seong H. Kim. His doctoral research focused on exploring the tribochemistry of hydrogenated diamond-like carbon coatings and their role in superlubricity. His work involved a variety of chemical characterizations, mechanical testing, and kinetic modeling to study these phenomena. Dr. Jang is currently a postdoctoral associate in the Surface Engineering and Tribology group within the Materials Science and Technology Division at Oak Ridge National Laboratory, where his research focuses on gaining a fundamental understanding and developing advanced coatings and EV fluid lubricants with enhanced tribological, thermal, and electrical properties using carbon nanotubes and ionic liquids.

Zhe Chen joined the School of Mechanical Engineering, Zhejiang University, China, in 2021 after completing postdoctoral research at Massachusetts Institute of Technology, USA, and The Pennsylvania State University, USA. He earned his Ph.D. degree in mechanical engineering from Tsinghua University, China, and his B.S. degree in mechanical engineering from Northwestern Polytechnical University, China. He was awarded Wen Shizhu Maple Leaf Award in 2022. His research interests include nanotribology, nanolubricants, and current-carrying friction.

Seong H. Kim joined the Faculty of Chemical Engineering at Penn State, USA, in 2001 after completing his Ph.D. study in Chemistry at Northwestern University, USA and conducting post-doctoral research at University of California, USA. He is currently a Distinguished Professor of Chemical Engineering and has courtesy appointments with the Department of Chemistry and the Department of Materials Science and Engineering at Penn State, USA. Dr. Kim's research interests lie in surface science and materials characterization. Since he moved to Penn State, he has established strong research programs which are all original: nanotribology and tribochemistry, surface science of silicate glass, and structure–property relationship of crystalline biopolymers in biological materials. Although these topics seem diverse and unrelated, Dr. Kim has identified and worked on scientific questions that require employing fundamental surface science principles and characterizations in these research fields. He has published more than 350 papers, and (based on Google Scholar) the *h*-index of his published work is 70. He recently finished writing a textbook on *Surface and Interface Analysis—Principles and Applications*, which is currently under production through Wiley and will come out in March 2025.